Iron(II) Complexes of Polydentate Aminopyridyl Ligands and an Exchangeable Sixth Ligand; Reactions with Peroxides. Crystal Structure of [FeL^1(H$_2$O)][PF$_6$]$_2$·H$_2$O [L^1 = *N,N'*-bis(6-methyl-2-pyridylmethyl)-*N,N'*-bis(2-pyridylmethyl)ethane-1,2-diamine]†

Ivan Bernal,[a] Inge Margrethe Jensen,[b] Kenneth B. Jensen,[b] Christine J. McKenzie,[b] Hans Toftlund[b] and Jean-Pierre Tuchagues[c]
[a] *Department of Chemistry, University of Houston, Houston, TX 77202.5641, USA*
[b] *Department of Chemistry, Odense University, DK-5230 Odense M, Denmark*
[c] *Laboratoire de Chemie de Coordination, CNRS, F-31077 Toulouse Cedex, France*

Iron(II) complexes of the pentadentate ligand *N*-methyl-*N,N',N'*-tris(2-pyridylmethyl)ethane-1,2-diamine (L^2) and the potentially hexadentate ligand *N,N'*-bis(6-methyl-2-pyridylmethyl)-*N,N'*-bis(2-pyridylmethyl)ethane-1,2-diamine (L^1) have been isolated. Both ligands behave as pentadentate ligands in their iron(II) complexes with the general formulation [FeL(X)]$^{n+}$ (L = L^1 or L^2, n = 1 or 2) with the sixth co-ordination site (X) occupied by an auxiliary ligand *e.g.* H$_2$O, Cl, SCN or CN. The crystal structure of [FeL^1(H$_2$O)][PF$_6$]$_2$·H$_2$O **1** shows that the nitrogen atom of one of the 6-methyl-2-pyridylmethyl groups of the formally hexadentate ligand is not co-ordinated to the iron atom. Instead a water molecule occupies the sixth co-ordination position. Complex **1** crystallizes in the triclinic space group $P\bar{1}$, with a = 10.485(2), b = 13.161(5), c = 14.853(6) Å, α = 69.31(4), β = 74.42(3), γ = 66.37(3)° and Z = 2. The structure refined to a final R value of 0.052 for 2531 reflections. The complexes show peroxidase activity, the availability of a labile site on the relatively stable iron(II) complexes, along with no apparent tendency to form oxo-bridged diiron(III) species, which are likely to be crucial factors in the mechanism of the oxidation reactions. Efforts to isolate a complex with a co-ordinated peroxide in the sixth position were unsuccessful. However, we have spectroscopic evidence that peroxide reacts with the iron(II) complexes to form an unstable species, probably of the form [Fe^{III}L(OOR)]$^{2+}$ (L = L^1 or L^2, R = H or Bu^t). The peroxide ligand in this iron(III) complex is likely to be forced into an 'end-on' co-ordination mode.

The study of the activation of H$_2$O$_2$ and O$_2$ by complexes of iron(II) may provide insight into the possible reaction modes of the iron-containing enzymes involved in oxygen activation, in particular the catalytic mechanisms of oxidases, peroxidases and oxygenases. We have been particularly interested in the oxygen activation mechanisms of the non-haem iron enzymes. Among these proteins are haemerythrin[1] and methane monooxygenase,[2] both of which contain a dinuclear active site, although oxygen co-ordination/activation is proposed to occur at only one of the iron atoms. By contrast a group of enzymes containing one non-haem iron centre at their active sites, mainly monooxygenases and dioxygenases, are important in the metabolism of fatty acids or aromatic compounds. The lipoxygenases catalyse the peroxidation of fatty acids with a 1,4-diene unit.[3] Catechol 1,2-dioxygenases function *via* an oxygen activation step by a mononuclear iron centre.[4] It is also well known that bleomycin is able to form a complex with iron which can activate molecular oxygen in a manner reminiscent of haem-bearing oxygenases and peroxidases. Recent work suggests that activated bleomycin incorporates dioxygen in the form of Fe^{III}-bound hydroperoxide in which the bleomycin provides five nitrogen donors.[5] The oxygen activation properties of mononuclear iron(II) complexes with a single labile co-ordination site are particularly relevant here in mimicking the properties of naturally occurring bleomycin, oxygenases and peroxidases.

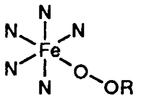

I

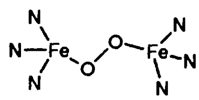

II

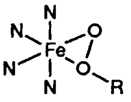

III

R = alkyl or H

In the present study we have investigated the use of pentadentate aminopyridyl ligands based on ethylenediamine. The sixth co-ordination site of the octahedral iron atom in these complexes is then occupied by a monodentate ligand and available for substitution reactions. This work prompted reactivity studies with peroxides. It was hoped that peroxo species with 'end-on' peroxide co-ordination (**I**, below) might be accessible by the addition of hydrogen peroxide or alkyl peroxides to iron(II) complexes with one labile co-ordination site. End-on co-ordination of hydroperoxide is the accepted mode of binding of reduced oxygen to one of the iron(III) atoms in oxyhaemerythrin and also in the haem-containing peroxidases. Such species are likely to be powerful oxidants. Our expectation was that the use of bulky pentadentate ligands may prevent the formation of the potentially 'dead-end' species, oxo-bridged diiron(III) complexes under oxidizing conditions.

---

† *Supplementary data available* (SUP 57106, 18 pp.): Mössbauer spectra and magnetic moments. See Instructions for Authors, *J. Chem. Soc., Dalton Trans.*, 1995, pp. xxv–xxx.

Non-SI unit employed: $\mu_B \approx 9.274 \times 10^{-24}$ J T^{-1}.

Studies related to this work have been carried out by Kitajima *et al.*[6] in which a short-lived peroxide adduct of the iron(II) complex of the tridentate hydrotris(3,5-diisopropylpyrazol-1-yl)borate $HB(C_3N_2HPr^i{}_2\text{-}3,5)_3$ ligand has been proposed to account for the spectroscopic results. Dioxygen was found to react at −20 °C with the five-co-ordinated complex $[Fe(O_2CPh)\{HB(C_3N_2HPr^i{}_2\text{-}3,5)_3\}]$ to give a dark green species with a band at *ca.* 680 nm in the electronic spectrum. Kitajima *et al.*[6] believe this unstable species is a peroxo-bridged binuclear product of type **II** depicted above. This assignment is based also on the dioxygen uptake ($Fe:O_2 = 2:1$), a resonance Raman enhanced O–O stretching vibration at 872 cm^{-1}, the intense absorption in the visible spectrum attributable to a peroxide-to-iron charge transfer, a Fe$\cdots$Fe distance of 4.3 Å [determined by extended X-ray absorption fine structure spectroscopy (EXAFS)] and some degree of antiferromagnetic coupling as determined by solution NMR spectroscopy ($J = -33$ cm^{-1}).

Que and co-workers[7] have worked with the iron(II) complexes of the tetradentate ligand, tris[(6-methyl-2-pyridyl)methyl]amine, tmpma. *tert*-Butyl hydroperoxide reacts at −60 °C with $[Fe(tmpma)(O_2CPh)]ClO_4$ giving an unstable pink species with a band at 510 nm in the electronic spectrum. η^2-Peroxide co-ordination is a likely candidate ('side-on' co-ordination, **III** above) for the structure of this peroxo adduct.

Some reports of the reactivity of iron(II) complexes and peroxides toward a number of potential substrates have been made in order to elucidate the mechanisms and species involved.[8] For example, the catalytic activity of iron(II) complexes of 1,4,8,11-tetraazacyclotetradecane (and related ligands) towards the epoxidation of olefins by hydrogen peroxide has been examined by Valentine and co-workers.[8b] An OOH^- complex of (1,4,8,11-tetraazacyclotetradecane)iron was postulated as a likely reactive intermediate.

Experimental

IR spectra were measured as KBr discs using a Hitachi 270-30 IR spectrometer. NMR spectra were recorded with a Bruker AC 250 FT NMR spectrometer. UV/VIS absorption spectra were recorded on a Shimadzu UV-3100 spectrophotometer. Electrospray mass spectra (ESMS) were obtained using a Finnigan TSQ 710 with a combined electrospray and atmospheric pressure chemical ionization source. Fast atom bombardment mass spectra (FABMS) were recorded on a KRATOS MS50TC. Cyclic voltammograms were recorded using a locally constructed three-electrode potentiostat. The working electrode was a BAS platinum electrode, the auxiliary electrode was a platinum wire, and the reference a BAS Ag–AgCl electrode. Elemental analyses were carried out at the microanalytical laboratory of the H. C. Ørsted Institute, Copenhagen. Electron spin resonance spectra were recorded at 77 K on a Varian E-LINE Century series spectrometer operating at the X-band.

Syntheses.—N,N′-*Bis*(6-*methyl*-2-*pyridylmethyl*)-N,N′-*bis*-(2-*pyridylmethyl*)*ethane*-1,2-*diamine* (L^1). This ligand was prepared after a modification of the method by Toftlund and Yde-Andersen.[9] First *N*,*N*′-bis(6-methyl-2-pyridylmethyl)-ethane-1,2-diamine was prepared by treating ethane-1,2-diamine (3.3 g, 50 mmol) with 6-methyl-2-pyridinecarbaldehyde (12.2 g, 100 mmol) in ethanol, followed by reduction with sodium borohydride, and the crude product was used without further purification. Under vigorous stirring an aqueous solution of 2-chloromethylpyridine hydrochloride (12.8 g, 100 mmol, 20 cm^3) was added dropwise to a mixture of the crude *N*,*N*′-bis(6-methyl-2-pyridylmethyl)ethane-1,2-diamine dissolved in dichloromethane (40 cm^3), aqueous sodium hydroxide (8.0 g, 200 mmol, 20 cm^3) and tetraethylammonium bromide (0.21 g, 0.001 mmol). The reaction mixture was stirred vigorously for another 9 days at 5 °C. The phases were separated and the aqueous phase was extracted twice with dichloromethane (2 × 50 cm^3). The combined organic phases were dried over sodium sulfate. The solvent was removed and the resulting oil was treated with boiling light petroleum (b.p. range 40–60 °C), to yield white crystals of L^1. Yield 11.2 g, 50%. NMR ($CDCl_3$): ^1H (250 MHz), δ 2.49 (CH_3 of pyridyl, s, 6 H), 2.77 (NCH_2CH_2N, s, 4 H), 3.76 (NCH_2 of pyridyl, s, 4 H), 3.78 (NCH_2 of pyridyl, s, 4 H) and 6.96–8.48 (pyridyl H, m, 14 H); $^{13}C\text{-}\{^1H\}$ (62.9 MHz), δ 24.25 (CH_3 of pyridyl), 52.22 (NCH_2CH_2N), 60.69, 60.77 (NCH_2 of pyridyl), 119.22, 121.08, 121.57, 122.44, 136.03, 136.32, 148.742, 157.258, 159.04 and 159.78 (pyridyl C).

N-*Methyl*-N,N′,N′-*tris*(2-*pyridylmethyl*)*ethane*-1,2-*diamine* (L^2). *N*-Methylethane-1,2-diamine (2.96 g, 40 mmol) dissolved in dichloromethane (50 cm^3) was mixed with a solution of 2-chloromethylpyridine hydrochloride (19.66 g, 120 mmol) in water (40 cm^3). The mixture was stirred under a dinitrogen atmosphere and aqueous sodium hydroxide (25 cm^3, 9.6 mol dm^{-3}) was added in small portions over a period of 24 h. The mixture was stirred a further 3 d after which time the phases were separated. The aqueous phase was extracted 3 times with CH_2Cl_2 (100 cm^3 portions) and the combined organic phases dried over sodium sulfate. The solution was filtered and the CH_2Cl_2 was removed on a rotary evaporator to leave L^2 as a dark red oil, sufficiently pure for complex formation. Yield of crude oil 13.78 g, 99%. NMR ($CDCl_3$): ^1H (250 MHz), δ 2.28 (NCH_3, s, 3 H), 2.77 (NCH_2CH_2N, m, 4 H), 3.70 (NCH_2 of pyridyl, s, 2 H), 3.90 (NCH_2 of pyridyl, s, 4 H) and 7.00–8.56 (pyridyl, m, 12 H). $^{13}C\text{-}\{^1H\}$ (62.9 MHz), δ 42.19, 51.55, 55.03, 60.27, 63.34, 121.38 (2 pyridyl C), 121.43 (1 pyridyl C), 122.37 (2 pyridyl C), 122.57 (1 pyridyl C), 135.82 (3 pyridyl C), 148.61 (2 pyridyl C), 148.69 (1 pyridyl C) and 159.21 (3 pyridyl C). Mass spectrum (EI): *m*/*z* 347 (M^+, 5%), 255 ($M^+ - CH_2C_5H_4N$, 16%), 212 [$M^+ - N(CH_3)CH_2C_5H_4N$, 100%], 135 [$M^+ - N(CH_2C_5H_4N)_2$, 44%] and 92 ($CH_2C_5H_4N^+$, 41%).

Aqua[N,N′-*bis*(6-*methyl*-2-*pyridylmethyl*)-N,N′-*bis*(2-*pyridylmethyl*)*ethane*-1,2-*diamine*]*iron*(II) *hexafluorophosphate*, $[FeL^1(H_2O)][PF_6]_2$ **1**. The salt $FeSO_4\cdot7H_2O$ (0.31 g, 1.1 mmol) was dissolved in methanol (5 cm^3) with iron turnings and one drop of 2 mol dm^{-3} H_2SO_4 and stirred at 50 °C and flushed with N_2 for *ca.* 10 min. The solution was filtered and added to a degassed solution of L^1 (0.50 g, 1.1 mmol) in methanol (5 cm^3) followed by ammonium hexafluorophosphate (0.35 g, 2.2 mmol). The solution was stirred, filtered and left to crystallize. Pale yellow-green microcrystalline $[FeL^1(H_2O)][PF_6]_2$ was isolated after standing for one day (0.42 g, 46%) (Found: C, 40.60; H, 4.10; N, 10.90. $C_{28}H_{34}F_{12}FeN_6OP_2$ requires: C, 41.20; H, 4.20; N, 10.30%). IR: 2930, 1608, 1576, 1465, 1440, 1085, 840 and 559 cm^{-1}.

Chloro[N,N′-*bis*(6-*methyl*-2-*pyridylmethyl*)-N,N′-*bis*(2-*pyridylmethyl*)*ethane*-1,2-*diamine*]*iron*(II) *hexafluorophosphate*, $[FeL^1Cl][PF_6]$ **2**. All solutions were flushed with N_2 for 10 min. Freshly prepared $FeCl_2\cdot2H_2O$ (0.194 g, 1.19 mmol) was dissolved in methanol (2 cm^3), and added to a solution of L^1 (0.515 g, 1.14 mmol) in methanol (5 cm^3). The resulting yellow-brown solution was stirred under dinitrogen and heated to 50 °C for approximately 10 min. Ammonium hexafluorophosphate [0.20 g, 1.23 mmol in methanol (2 cm^3)] was added and the mixture was filtered. Yellow crystals deposited on standing. These were collected after approximately 30 min and were washed with methanol (0.446 g, 60%) (Found: C, 49.50; H, 4.80; Cl, 6.60; N, 11.75. $C_{28}H_{32}ClF_6FeN_6P$ requires C, 48.80; H, 4.70; Cl, 5.15; N, 12.20%). FAB MS: *m*/*z* 543.4 ($[FeL^1Cl]^+$, 25%). IR: 2925, 1606, 1574, 1462, 1442, 844 and 559 cm^{-1}.

[N,N′-*Bis*(6-*methyl*-2-*pyridylmethyl*)-N,N′-*bis*(2-*pyridylmethyl*)*ethane*-1,2-*diamine*]*thiocyanatoiron*(II) *hexafluorophosphate*, $[FeL^1(SCN)]PF_6$ **3**. The complex $[FeL^1(H_2O)][PF_6]_2$ (0.20 g, 0.25 mmol) was dissolved in methanol (10 cm^3)–water (1 cm^3) and an excess of Na(SCN) (0.20 g, 2.5 mmol) was added and the solution was stirred and filtered. Yellow crystals deposited over 2 d, and these were collected and washed with methanol (0.117 g, 65%) (Found: C, 48.30; H, 4.75; N, 13.25; S, 4.75. $C_{29}H_{32}F_6FeN_7PS$ requires C, 48.95; H, 4.55; N, 13.80; S, 4.50%). FAB MS: *m/z* 566.4 ($[FeL^1(SCN)]^+$, 15%). IR: 2927, 2055, 1651, 1606, 1574, 1462, 1442, 844 and 559 cm^{-1}.

Chloro[N-*methyl*-N,N′,N′-*tris*(2-*pyridylmethyl*)*ethane*-1,2-*diamine*]*iron*(II) *hexafluorophosphate*, $[FeL^2Cl]PF_6$ **4**. The following synthesis was carried out under argon using standard Schlenk techniques. Freshly prepared $FeCl_2{\cdot}2H_2O$ (0.445 g, 2.7 mmol) was added to a solution of L^2 (0.728 g, 2.1 mmol) in dry methanol (20 cm^3). The resulting yellow-brown solution was stirred for 15 min after which time ammonium hexafluorophosphate (0.828 g, 5.1 mmol) was added. The yellow-green crystals deposited were collected and washed with methanol. Recrystallization was carried out by slow evaporation of a solution of the complex in acetone–ethanol (0.487 g, 40%) (Found: C, 42.10; H, 4.35; Cl, 6.70; N, 11.75. $C_{21}H_{25}ClF_6FeN_5P$ requires: C, 43.20; H, 4.30; Cl, 6.05; N, 12.00%). FAB MS: *m/z* 438.1 ($[FeL^2Cl]^+$, 100%).

Table 1 Summary of data collection and processing parameters for $[FeL^1(H_2O)][PF_6]_2{\cdot}H_2O$ **1**

Molecular formula	$C_{28}H_{36}F_{12}FeN_6O_2P_2$
M	833.79
Space group	$P\bar{1}$ (no. 2)
a/Å	10.485(2)
b/Å	13.161(5)
c/Å	14.853(6)
α/°	69.31(4)
β/°	74.42(3)
γ/°	66.37(3)
U/Å^3	1725.54
Z	2
D_c/g cm^{-3}	2.061
Radiation (λ/Å)	Mo-Kα (0.710 73)
μ/cm^{-1}	6.2
Relative transmission coefficients	0.9535–0.9983
Data collection range/°	$4 \leqslant 2\theta \leqslant 45$
Scan width	$0.95 + 0.35 \tan\theta$
Total data collected	3629
Data used in refinement *	2531
$R = \Sigma\|\|F_o\| - \|F_c\|\|/\Sigma\|F_o\|$	0.052
$R' = [\Sigma w^2(\|F_o\| - \|F_c\|)^2/\Sigma\|F_o\|^2]^{\frac{1}{2}}$	0.067
Weighting, w	$[\sigma(F_o)]^{-2}$

* The difference between this number and the total is due to subtraction of 1098 data that were redundant and collected to obtain reflections suitable for the absorption correction, symmetry related, standards or did not meet the criterion of $I \geqslant 3\sigma(I)$.

X-Ray Crystallography.—Crystals of $[FeL^1(H_2O)][PF_6]_2{\cdot}H_2O$ **1** suitable for X-ray diffraction studies were grown by slow evaporation of a solution of the complex in water–acetonitrile (1 : 1). Intensity data were collected with an Enraf-Nonius CAD-4 diffractometer operating with a Molecular Structure Corporation TEXRAY-230 modification[10] of the SDP-Plus software package.[11] The crystal was centred with data in the range $20 \leqslant 2\theta \leqslant 36°$ and examination of the cell constants, absences, and Niggli matrix 1[12] showed **1** to crystallize in the space groups $P1$ or $P\bar{1}$ which are not unambiguously defined. However, since $Z = 2$, the centrosymmetric space group was chosen first, and eventually found to be correct. Details of the data collection and processing are summarized in Table 1. The intensity data were corrected for absorption using empirical curves derived from ψ-scans[10,11] of suitable reflections. The scattering curves were taken from Cromer and Waber's compilation.[13] During data collection intensity and orientation standards were monitored and showed no significant deviations from the initial values.

The structure was solved by the Patterson method, and refined using the PC version of the NRCVAX Program Package.[14] Heavy atoms were refined anisotropically until convergence and hydrogen atoms of the cations were added at fixed, idealized positions (N–H, C–H = 0.95 Å; B = 5.0 Å^2). Hydrogens of water were found in a late difference map and added as fixed contributions at the positions found (B = 5.0 Å^2, fixed) to the final cycle. Final $R(F)$ and $R'(F)$ factors are listed in Table 1. The contents of the asymmetric unit are shown in Fig. 1 and a packing diagram of the ions and the waters of crystallization are shown in Fig. 2. Final positional parameters

Table 2 Atomic coordinates for the non-hydrogen atoms of $[FeL^1(H_2O)][PF_6]_2{\cdot}H_2O$ **1**

Atom	*x*	*y*	*z*
Fe	0.295 57(12)	0.155 19(8)	0.240 28(7)
P(1)	0.042 8(3)	0.225 58(19)	0.739 83(16)
P(2)	0.650 0(3)	0.445 21(21)	0.209 66(16)
F(1)	−0.078 2(8)	−0.130 6(5)	0.164 9(4)
F(2)	0.199 7(9)	0.203 5(9)	0.694 1(6)
F(3)	0.055 1(12)	0.312 3(6)	−0.217 3(5)
F(4)	0.889 8(9)	0.256 6(11)	−0.212 9(6)
F(5)	0.033 3(13)	0.142 4(6)	0.696 0(6)
F(6)	0.005 7(7)	0.321 8(5)	0.643 7(4)
F(7)	0.720 6(11)	0.318 5(5)	0.244 5(7)
F(8)	0.337 3(7)	0.561 3(7)	−0.104 1(4)
F(9)	0.199 4(7)	0.540 4(6)	−0.173 9(4)
F(10)	−0.366 1(7)	0.462 8(7)	0.311 5(4)
F(11)	0.499 8(7)	0.431 3(8)	0.246 2(5)
F(12)	0.419 2(8)	0.422 1(5)	−0.171 8(5)
O(w1)	0.246 5(5)	0.025 6(3)	0.332 9(3)
O(w2)	0.072 7(8)	−0.074 4(5)	0.437 6(6)
N(1)	0.483 4(7)	0.120 2(5)	0.125 3(4)
N(2)	0.280 4(7)	0.326 3(5)	0.130 3(4)
N(3)	0.155 8(7)	0.277 2(4)	0.336 6(4)
N(4)	0.435 9(8)	0.144 8(5)	0.332 9(4)
N(5)	0.142 3(7)	0.178 0(5)	0.154 8(4)
N(6)	−0.167 9(7)	0.306 2(5)	0.499 3(4)
C(1)	0.520 8(9)	0.214 1(6)	0.069 8(5)
C(2)	0.634 8(10)	0.208 0(7)	−0.007 1(6)
C(3)	0.716 4(10)	0.103 8(9)	−0.025 9(6)
C(4)	0.680 7(11)	0.008 1(8)	0.031 3(7)
C(5)	0.566 1(9)	0.017 7(6)	0.105 3(5)
C(6)	0.522 6(10)	−0.085 1(7)	0.170 4(6)
C(7)	0.428 3(10)	0.323 2(6)	0.098 0(5)
C(8)	0.185 9(8)	0.420 0(6)	0.178 3(5)
C(9)	0.192 3(8)	0.384 1(6)	0.286 0(5)
C(10)	0.205 0(10)	0.221 9(6)	0.431 1(5)
C(11)	0.363 2(9)	0.176 3(6)	0.416 7(5)
C(12)	0.432 3(11)	0.161 8(7)	0.489 0(6)
C(13)	0.578 4(12)	0.117 4(7)	0.473 1(6)
C(14)	0.652 8(10)	0.087 6(7)	0.386 6(7)
C(15)	0.575 8(11)	0.102 2(7)	0.320 1(6)
C(16)	0.224 9(9)	0.334 6(6)	0.047 0(5)
C(17)	0.127 9(9)	0.266 3(6)	0.074 6(5)
C(18)	0.033 8(10)	0.288 8(7)	0.016 1(6)
C(19)	−0.046 1(10)	0.220 4(9)	0.038 2(7)
C(20)	−0.032 6(10)	0.130 3(8)	0.121 0(7)
C(21)	0.061 3(9)	0.112 1(6)	0.177 2(5)
C(22)	0.006 0(9)	0.291 1(6)	0.347 0(5)
C(23)	−0.103 1(8)	0.362 1(6)	0.414 2(5)
C(24)	−0.148 8(10)	0.479 7(6)	0.391 7(6)
C(25)	−0.252 9(12)	0.536 2(7)	0.456 1(9)
C(26)	−0.315 8(11)	0.478 3(9)	0.540 4(8)
C(27)	−0.273 3(10)	0.360 7(8)	0.562 7(6)
C(28)	−0.340 8(12)	0.288 0(9)	0.651 0(7)
H(w1)	0.176	−0.018	0.381
H(w2)	0.313	−0.003	0.324
H(w3)	0.055	0.005	0.447
H(w4)	0.138	−0.095	0.495

for the non-hydrogen atoms are given in Table 2. Distances, angles and selected torsional angles are listed in Table 3.

Additional material available from the Cambridge Crystallographic Data Centre comprises H-atom coordinates, thermal parameters and remaining bond lengths and angles.

Magnetic Susceptibility Measurements.—Variable-temperature magnetic susceptibility data were obtained on powdered polycrystalline samples with a Quantum Design MPMS SQUID susceptometer. Diamagnetic corrections were applied by using Pascal's constants.

Mössbauer Spectra.—Mössbauer measurements were obtained on a constant-acceleration conventional spectrometer with a 25 mCi source of ^{57}Co (Rh-matrix). Isomer shift values (δ) throughout the paper are given with respect to metallic iron at room temperature. The absorber was a sample of 120 mg of microcrystalline powder enclosed in a 2 cm diameter cylindrical plastic sample holder, the size of which had been determined to optimize the absorption. Variable-temperature spectra were obtained in the range 300–80 K, by using a MD 306 Oxford cryostat, the thermal scanning being monitored by an Oxford ITC4 servocontrol device (± 0.1 K accuracy). A least-squares computer program [15] was used to fit the Mössbauer parameters and determine their standard deviations of statistical origin (given in parentheses).

Peroxidase Activity Experiments.—(*a*) *Oxidation of* abts [*2,2′-azinobis(3-ethylbenzothiazoline-6-sulfonic acid)*]. In a typical experiment abts, the iron complex and a buffer were mixed in a cuvette. The experiment was initiated by addition of hydrogen peroxide. The oxidation of abts was followed by the change in absorption at 418 nm due to abts$^{\bullet+}$ on a Shimadzu UV/VIS 160 Recording Spectrophotometer. A turnover after 80 s was taken as a measure of catalytic activity. The ratio substrate : oxidant : catalyst was 1000 : 2000 : 1, the concentration of the substrate was 1.5 mmol dm^{-3}, and the total volume was 1.325 cm^3. An absorption coefficient of 3.24×10^4 dm^3 mol^{-1} cm^{-1} for abts$^{\bullet+}$ was used.[16]

(*b*) *Oxidation of* 4-*methoxybenzyl alcohol.* In a typical experiment the substrate, the iron complex and hydrogen peroxide were mixed with water. The ratio substrate : hydrogen peroxide : catalyst was 70 : 35 : 1, the concentration of the substrate was 13 mmol dm^{-3}, and the total volume was 2.7 cm^3. After 4 and 24 h of reaction 1 cm^3 samples were taken. Acetophenone was added to the sample as an internal standard, water was added and the samples were extracted with dichloromethane and analysed by GC. Gas chromatography was performed with a Carlo Erba/Kratos MFC 500 instrument equipped with a HP-5 capillary column and a FID. Products were identified by comparison with authentic samples.

Results and Discussion

Syntheses.—The syntheses of the potentially hexadentate ligand *N*,*N*′-bis(6-methyl-2-pyridylmethyl)-*N*,*N*′-bis(2-pyridylmethyl)ethane-1,2-diamine (L^1) and the pentadentate ligand *N*-methyl-*N*,*N*′,*N*′-tris(2-pyridylmethyl)ethane-1,2-diamine (L^2) together with some of their iron(II) complexes **1**–**4**, are presented in the Experimental section. The reaction of L^1 with $[Fe(H_2O)_6]^{2+}$ gave, instead of the expected $[FeL^1][PF_6]_2$ in which the ligand is hexadentate by co-ordination *via* the two $NC_5H_4CH_2$ nitrogen atoms, the two $NC_5H_3(Me)CH_2$ nitrogen atoms and the two amino nitrogen atoms, a complex, in which, according to its X-ray structure, the ligand acts as a pentadentate donor with one of the $NC_5H_3(Me)CH_2$ arms unco-ordinated, see below. The structure shows that the complex can be formulated as $[FeL^1(H_2O)][PF_6]_2$ **1**, with a water molecule in the sixth position of the octahedral iron(II). Attempts to isolate an analogous complex with an aqua ligand in the sixth position with the deliberately designed pentadentate ligand L^2 were unsuccessful. However the analogous complexes, $[FeL^1Cl]PF_6$ **2** and $[FeL^2Cl]PF_6$ **4** were prepared by the reaction of the respective ligands with iron(II) chloride under an inert atmosphere. The aquo complex **1** and the chloro complexes **2** and **4** can be used for subsequent substitution reactions in which, for example, the aqua/chloro ligands are exchanged for thiocyanate or cyanide. One of these complexes, namely $[FeL^1(NCS)]PF_6$ **3**, was isolated and characterized. Others, $[FeL^2(NCS)]PF_6$ **5**, $[FeL^1(CN)]PF_6$ **6** and $[FeL^2(CN)]PF_6$ **7**, were identified in solution by UV/VIS spectroscopy and mass spectrometry. Red-brown solid products were obtained from the attempts to isolate the cyanide complexes **6** and **7**, however these are so far not well characterized. The aqua, chloro and thiocyanate complexes **1**–**4** were used in the reactions with hydrogen peroxide and *tert*-butyl hydrogen peroxide and the catalysis experiments described below. The UV/VIS spectrosopic and the redox properties of the $[FeL(X)][PF_6]_n$ ($L = L^1$ or L^2; $X = H_2O$, Cl, NCS or CN; $n = 1$ or 2) complexes are listed in Table 4.

Crystal and Molecular Structure of $[FeL^1(H_2O)][PF_6]_2\cdot H_2O$.—The crystal structure consists of cations hydrogen bonded to one of the PF_6^- counter anions *via* a water molecule and an isolated PF_6^- ion. The most interesting stereochemical result derived from the crystallographic study is the fact that one of the $NC_5H_3(Me)CH_2$ moieties is pendant, leaving one of the octahedral positions open to the attachment of a water molecule at this site. The contents of the asymmetric unit of $[FeL^1(H_2O)][PF_6]_2\cdot H_2O$ together with the atomic arrangement and numbering scheme are shown in Fig. 1 which depicts also the anions in the

Table 3 Selected bond distances (Å) and angles (°) for $[FeL^1(H_2O)][PF_6]_2\cdot H_2O$ **1**

Fe–O(w1)	1.919(4)	O(w1)–H(w1)	1.049(4)
Fe–N(1)	2.192(6)	O(w1)–H(w2)	0.641(5)
Fe–N(2)	2.244(6)	O(w2)–H(w1)	1.452(7)
Fe–N(3)	2.289(6)	O(w2)–H(w3)	1.044(7)
Fe–N(4)	2.237(7)	O(w2)–H(w4)	1.138(9)
Fe–N(5)	2.205(6)		
O(w1)–Fe–N(1)	117.5(3)	N(1)–Fe–N(5)	96.0(2)
O(w1)–Fe–N(2)	162.0(3)	N(2)–Fe–N(3)	79.3(2)
O(w1)–Fe–N(3)	93.4(2)	N(2)–Fe–N(4)	102.3(2)
O(w1)–Fe–N(4)	91.4(2)	N(2)–Fe–N(5)	75.9(2)
O(w1)–Fe–N(5)	89.4(2)	N(3)–Fe–N(4)	74.7(3)
N(1)–Fe–N(2)	75.1(3)	N(3)–Fe–N(5)	100.2(2)
N(1)–Fe–N(3)	145.3(2)	N(4)–Fe–N(5)	174.8(2)
N(1)–Fe–N(4)	88.3(2)		

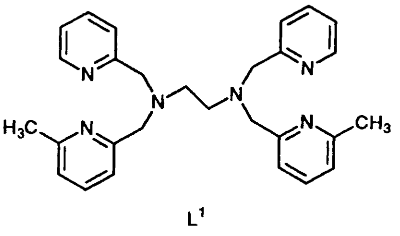

L^1

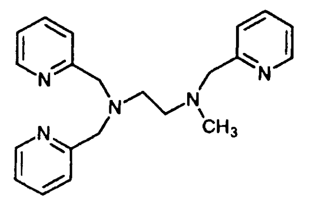

L^2

Table 4 UV/VIS spectroscopic and cyclic voltammetry data in acetonitrile for complexes $[FeL(X)][PF_6]_n$ ($L = L^1$ or L^2; $X = H_2O$, Cl, NCS or CN; $n = 1$ or 2)

Complex	UV/VIS λ_{max}/nm (ε/dm^3 mol^{-1} cm^{-1})	CV[a] E_{ox}/V	CV[a] E_{red}/V
1 $[FeL^1(H_2O)][PF_6]_2$	362 (1600)	0.71	0.62
	750 (20)		
	802 (9)		
2 $[FeL^1Cl]PF_6$	310 (1100)	0.70	0.64
	386 (1700)		0.28
	551 (12)		
	913 (7)		
4 $[FeL^2Cl]PF_6$	320 (935)	0.66	0.57
	399 (1840)		0.40
	571 [18 (sh)]		
	930 (14)		
3 $[FeL^1(NCS)]PF_6$	290 [2000 (sh)]	0.77	0.69
	385 (1900)		0.46
	541 (53)		
	866 (9)		
	1077 (7)		
5 $[FeL^2(NCS)]PF_6$[c]	398 (1500)		
	585 [69 (sh)]		
	882 (2)		
6 $[FeL^1(CN)]PF_6$[b]	332 [1200 (sh)]	0.74	0.61
	441 (6000)		
7 $[FeL^2(CN)]PF_6$[c]	343 [1300 (sh)]	0.66	0.59
	450 (8700)		

[a] *vs.* Ag–AgCl reference electrode. [b] The complex is characterized only in solution by adding 1 equivalent of NaCN to the corresponding chloro or aqua complex to obtain the UV/VIS spectra and 20 equivalents for the CV measurement. [c] The complex is characterized only in solution by adding 1 equivalent of the sodium salts of SCN^- or CN^- in aqueous solution to the acetonitrile solution of $[FeL^2Cl]PF_6$.

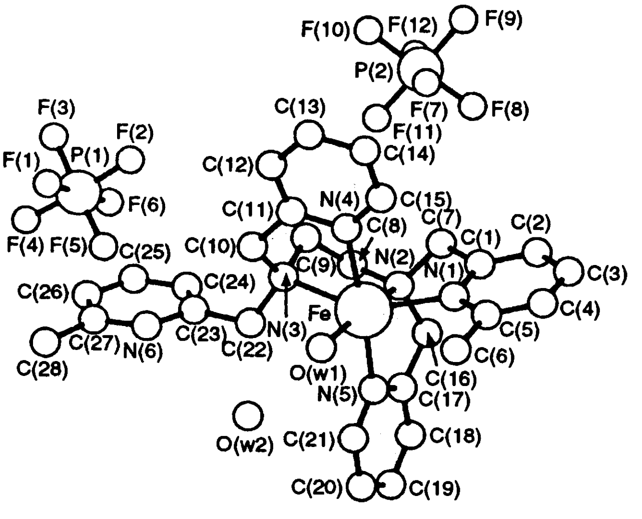

Fig. 1 The contents of the asymmetric unit consisting of a $[FeL^1(H_2O)]^{2+}$ cation, two PF_6^- anions and one water of crystallization. The anions and the water of crystallization were placed at those symmetry positions at which they have their shortest contacts with the cation. Note the locations of the anions with respect to the pyridine groups of the cation, particularly that of P(1) with respect to the dangling $NC_5H_3(Me)CH_2$ fragment and that of P(2) with respect to the pyridine group defined by N(4)–C(11) ··· C(15)

positions nearest to the cation. The water of crystallization, which is close to both the ligating water [hydrogen bonded to H(w1)] and N(6) of the pendant $NC_5H_3(Me)CH_2$ arm is also included in the figure. Selected bond distances and angles for $[FeL^1(H_2O)][PF_6]_2 \cdot H_2O$ are given in Table 3. The fact that the potentially hexadentate ligand binds the metal ion in a pentadentate fashion can be contrasted to the iron(II) complex of tetrakis(2-pyridylmethyl)ethanediamine (tpen),[17] in which the ligand is co-ordinated to the iron atom *via* all six of the nitrogen donors. The additional bulk provided by the methyl groups in the α positions of two of the NC_5H_3Me rings of L^1 compared to tpen is apparently enough to favour co-ordination of a water molecule instead of co-ordination of the second NC_5H_3Me group.

The co-ordination geometry around the iron atom deviates significantly from an ideal octahedral symmetry due to the fusion of the four five-membered chelate rings. The co-ordination of a water molecule instead of the second $NC_5H_3(Me)CH_2$ arm seems to release some of the meridional strain in the ethylenediamine plane. The angle between the two *trans* nitrogen atoms in the equatorial plane [N(3) and N(1)] is as low as 145.3(2)°, whereas the corresponding axial NC_5H_4 nitrogen atoms [N(4) and N(5)] are much closer to a linear arrangement [174.8(2)°]. Despite the strain, the co-ordinated $NC_5H_3(Me)$ nitrogen is closer [2.192(6) Å] to the iron atom than the two NC_5H_4 nitrogen atoms ($Fe-N_{av}$ = 2.221 Å). The $Fe-N(NC_5H_4)$ distances are slightly elongated compared to similar high-spin iron(II) complexes, whereas the distances to the aliphatic nitrogen atoms are significantly longer than the values reported for high-spin $[Fe(C_6H_8N_2)_3]Cl_2$ systems ($C_6H_8N_2$ = 2-pyridylmethylamino ligand).[18,19]

A most remarkable feature of the structure is the unusually short Fe–O(w1) distance to the terminal water of 1.919(4) Å. This distance is about 0.2 Å shorter than in other structures containing water bound to Fe^{II}[20] and even shorter than typical $Fe^{III}-OH_2$ distances. One of the reasons for the short Fe–O(w1) bond might be the interaction with the lattice water which is bridging between the pendant NC_5H_3Me nitrogen atom and H(w1) of the ligating water. A tautomeric form of this hydrogen-bonded network corresponds to a deprotonation of the ligated water. Another explanation might be that all the nitrogen atoms apparently function as rather poor σ donors in the present complex.

Hexafluorophosphate anions frequently exhibit large amplitudes of librational motion, however the thermal parameters of the two PF_6^- anions seem to be smaller than in the structures of many other PF_6^- salts. It is interesting that they are located close to the π clouds of the pyridine rings. For example, Fig. 1 shows that F(5) is in close proximity to the C(24)C(25)C(26) fragment as well as near H(28), and F(11) is close to C(13) and C(14), as well as H(17). Each PF_6^- ion is in close proximity to a dangling $NC_5H_3(Me)CH_2$ ring of one cation [*e.g.* F(5) ··· N(6) 3.76, F(5) ··· C(27) Å] and the pyridine rings of an adjacent cation [*e.g.* F(6) ··· C(10) 3.58; F(2) ··· C(5) 3.66, F(4) ··· C(2) 3.55 Å]. These contacts may have immobilized the PF_6^- anion and prevented some of the large thermal motion. A view of these pyridine–PF_6^- anion interactions is shown in the packing diagram (Fig. 2).

Electronic Spectra.—The UV/VIS spectra of the complexes **1**–**7** were recorded in acetonitrile. The spectrum of **5** was obtained by adding 1 equivalent of sodium thiocyanate to **4**, the spectra of **6** and **7** by addition of 1 equivalent of sodium cyanide to compound **2** or compound **4**, respectively. Identical spectra of **3** were obtained for solutions of the isolated compound and for substitution of chloride in solutions of **2** with thiocyanate anion. The data for the electronic spectra are summarized in Table 4. The UV/VIS spectra are dominated by the metal-to-ligand charge-transfer (m.l.c.t) band. The position and intensity of this band demonstrates complexes **1**–**5** to be high spin, and the cyanide complexes **6** and **7** to be low spin. The m.l.c.t. band is found at 362 nm for **1**, and it is seen to be red-shifted when a charged ligand is introduced, *e.g.* chloride or thiocyanate (386 and 385 nm). This shift reflects the influence of the exogenous ligand on the metal centre in the charge-transfer transition, which occurs at lower energy because the formal oxidation state

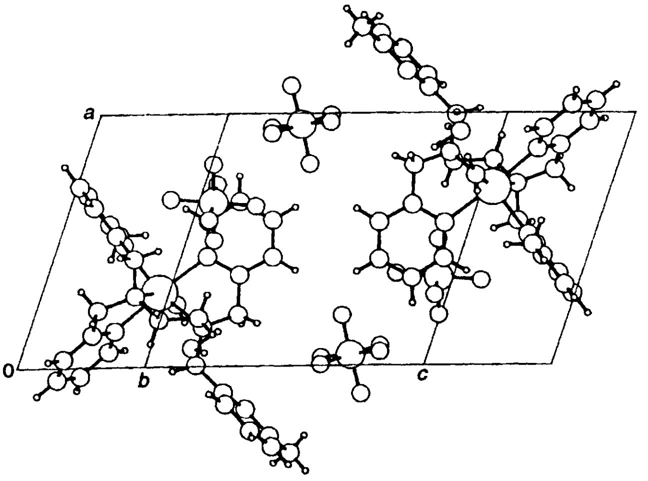

Fig. 2 The contents of the unit cell. Note the inversion centre at $\frac{1}{2}, \frac{1}{2}, \frac{1}{2}$ which relates pairs of cations, anions and waters of crystallization. Also note positions of the PF_6^- anions [P(1)] with respect to the dangling NC_5H_3Me rings and those of the PF_6^- anions [P(2)] with respect to the pyridine group defined by N(4)–C(11) ··· C(15)

of iron is lowered when the exogenous ligand is a better σ donor.[21] The m.l.c.t. bands for the iron(II) complexes of L^2 with chloride (**4**) and thiocyanate (**5**) are found at 399 and 398 nm, respectively. As for the corresponding L^1 complexes, the position of the band is not affected much in going from chloride to thiocyanate, indicating that it is the charge rather than the chemical nature of the exogenous ligand that determines the position of the band. For the high-spin complexes the $^5E_g \longleftarrow {}^5T_{2g}$ transition is observed as a low intensity band above 800 nm. This band is red shifted for the chloro and the thiocyanato complexes of both ligands. As expected, the ligand-field transitions for the chloro complexes are found at lower energy than the thiocyanato complexes for both ligands, since thiocyanate has a higher ligand-field strength.

When the exogenous ligand is cyanide, the iron(II) complexes are in the low-spin state, with a m.l.c.t. band at 441 nm for the L^1 complex **6** and 450 nm for the L^2 complex **7**. The $^1T_{1g} \longleftarrow {}^1A_{1g}$ ligand-field transitions for the cyanide complexes are most likely obscured by these intense charge-transfer bands.

The charge-transfer band of the aqua complex **1** is red-shifted to 400 nm if 2 equivalents of base (NEt_3) is added, resembling the spectra of the complexes containing other charged exogenous ligands (Cl, NCS, CN). This suggests that the co-ordinated water molecule can be deprotonated to hydroxide upon addition of base. The deprotonation appears to be reversible, and even after addition of six-fold excess of base, the 362 nm band of the original complex can be restored upon addition of six equivalents of perchloric acid accompanied by disappearance of the 400 nm band of the deprotonated species.

Electrochemistry.—Cyclic voltammograms were recorded of complexes **1**–**7** in acetonitrile. The potentials *vs.* the Ag–AgCl electrode are listed in Table 4. Reversible oxidation waves were observed at about 0.7 V for all complexes, *i.e.* the exogenous ligands have little effect on the oxidation potential. The relatively high potentials are consistent with the observed stability of the iron(II) complexes towards oxidation. The voltammograms of **2**, **3** and **4** featured a second reduction peak at lower potential. The cyclic voltammogram of **2** is presented in Fig. 3. We suggest that this second reduction peak might be due to a species formed in a chemical reaction taking place after the oxidation, or to the exchange of chloride or thiocyanate with a solvent molecule in either the reduced or oxidized complexes. Attempts to elucidate the origin of the second reduction wave by changing the solvent from acetonitrile to the non-coordinating solvent dichloromethane, or by adding a surplus of the exogenous ligand, were inconclusive.

Table 5 Representative least-squares fitted Mössbauer data for complexes **1**–**4***

T/K	Complex	**1**	**2**	**3**	**4**
293	δ	0.959(2)	0.952(1)	0.983(3)	0.953(4)
	ΔE_Q	2.423(5)	2.838(2)	1.435(7)	2.740(7)
	Γ/2	0.131(4)	0.120(2)	0.129(5)	0.123(6)
220	δ	1.006(3)	1.009(2)	1.020(2)	0.980(2)
	ΔE_Q	2.536(5)	2.982(3)	1.656(3)	2.986(3)
	Γ/2	0.129(4)	0.124(3)	0.126(3)	0.122(3)
150	δ	1.043(2)	1.048(2)	1.058(4)	1.015(1)
	ΔE_Q	2.600(2)	3.079(4)	1.938(8)	3.121(3)
	Γ/2	0.130(2)	0.120(3)	0.131(6)	0.120(2)
80	δ	1.061(1)	1.094(1)	1.090(1)	1.044(2)
	ΔE_Q	2.651(1)	3.118(3)	2.208(2)	3.186(4)
	Γ/2	0.132(1)	0.125(2)	0.134(1)	0.121(3)

* δ = Isomer shift (mm s^{-1}), ΔE_Q = quadrupole splitting (mm s^{-1}), Γ/2 = half width (mm s^{-1}); statistical standard deviations are given in parentheses.

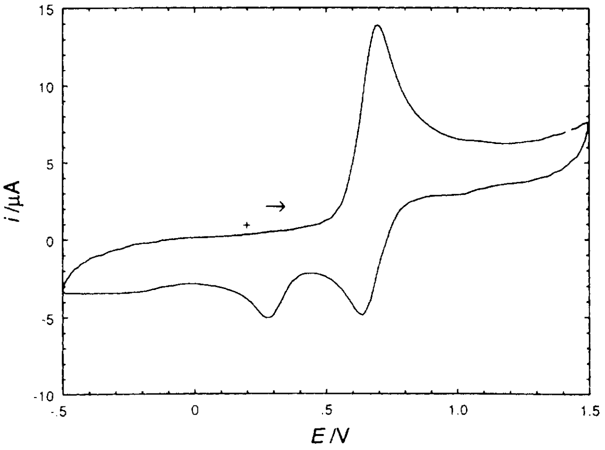

Fig. 3 The cylic voltammogram of $[FeL^1Cl]PF_6$ in acetonitrile (electrolyte NBu_4PF_6, scan rate 0.1 V s^{-1}) *vs.* Ag–AgCl

Magnetic Susceptibility.—The molar magnetic moments of powdered samples of complexes **1**–**4** determined in the 300–2 K temperature range have been determined. The effective magnetic moment per iron at 300 K is close to the spin-only value of 4.9 μ_B for $S = 2$ as usually observed for high-spin iron(II) complexes[22] (**1** 4.84 μ_B, **3** 4.80 μ_B) or slightly higher (**2** 4.98 μ_B, **4** 5.05 μ_B). The relatively small dependence of the magnetic moment of complexes **1**–**4** with temperature indicates that none of these complexes experiences noticeable magnetic exchange interactions. The decrease in their magnetic moment is situated between 20 and 2 K further indicating the presence of zero-field splitting of the high-spin iron(II) ground state. This conclusion agrees well with the results of the X-ray structural determination which shows complex **1** to be an isolated mononuclear species in which the iron is surrounded by ligands affording a distorted octahedral co-ordination sphere and showing that the shortest Fe ··· Fe distances are 8.607 Å. A listing of the effective magnetic moments over the measured temperature range is available as supplementary material (SUP 57106).

Mössbauer Spectroscopy.—The Mössbauer spectra of complexes **1**–**4** recorded at 293, 220, 150 and 80 K consist of a single quadrupole split doublet (SUP 57106). They were least-squares fitted to Lorentzian line shapes and the resulting isomer shift (δ) and quadrupole splitting parameters (ΔE_Q) are listed in Table 5. The δ and ΔE_Q values for the four complexes clearly indicate the presence of high-spin iron(II) in a distorted octahedral ligand environment. The δ values are weakly temperature dependent due to second-order Doppler shift.[23] Taking into account the relative ligand-field strengths and σ-donor ability of H_2O, Cl^- and SCN^- (see discussion of electronic spectra), the isomer shift values for complexes **1**–**4** are in the range expected for N_5O (**1**), N_5Cl (**2**, **4**) and N_6 (**3**) ligand environments, although in the lower end.[23,24]

The molecular structure of $[FeL^1(H_2O)][PF_6]_2$ **1** indicates that the distortion of the octahedral geometry is essentially rhombic including an axial compression along $O(w1) \cdots N(2)$ (C_4 axis). Consequently, the ground state must be the $|xy\rangle$ orbital singlet. The low-temperature ΔE_Q value (2.65 mm s^{-1} at 80 K) is about 33% lower than the maximum value of 4 mm s^{-1} expected for an isolated singlet ground state.[25] This can be attributed to the effect of the spin–orbit interaction. A complementary explanation also supported by the small isomer shift values is that covalency effects have reduced the ΔE_Q values. The 2.42–2.65 mm s^{-1} ΔE_Q variation in the 293–80 K temperature range indicates that the energy separation D_s between the singlet ground state and the higher orbital states is too large to allow significant thermal population of the higher orbital states at 293 K. It is possible roughly to assess this energy separation assuming that the ΔE_Q slope varies as D_s^{-1}.[26] The slope $d\Delta E_Q/dT$ can be determined by linear regression as 1.24×10^{-3} mm s^{-1} K^{-1} and comparison with the $d\Delta E_Q/dT$ slope determined for ^{57}Fe doped K_2ZnF_4[26] yields a rough estimate of ≈ 1300 cm^{-1} for D_s for complex **1**.

Although similar comments can be made for $[FeL^1Cl]PF_6$ **2** in view of its ΔE_Q value and temperature dependence, the nature of the ground state orbital singlet is not known as crystallographic data are not available. However, the large energy separations between the singlet ground state and higher orbital states (990 cm^{-1}) indicates also a large D/λ ratio for **2**.

For $[FeL^1(SCN)]PF_6$ **3**, the ΔE_Q value of 2.21 mm s^{-1} at 80 K and its strong temperature dependence indicate that the energy separation between the ground state and the first higher orbital state is small enough to result in a significant thermal population of the latter even at low temperature. Actually, this energy separation of 474 cm^{-1} can be assessed more precisely for complex **3** than for **1** and **2** due to comparable values of the $d\Delta E_Q/dT$ slope for **3** and ^{57}Fe doped K_2ZnF_4. For such small orbital level separations, the role of the spin–orbit coupling becomes very important and an understanding of the system would require much more elaborate studies which are beyond the scope of this paper.

The low-temperature ΔE_Q value is relatively large for $[FeL^2Cl]PF_6$ **4** indicating that the T_{2g} orbital triplet is split by crystal-field distortions affording lower than octahedral symmetry and that the lower state is an orbital singlet. Decrease of ΔE_Q at room temperature indicates an energy separation (assessed as indicated above) of 488 cm^{-1} and the presence of excited T_{2g} thermally accessable levels in this complex. The low-temperature ΔE_Q value (about 30% lower than the maximum value of 4 mm s^{-1} expected for an isolated singlet ground state[26]) can be attributed to the effect of the spin–orbit interaction. Actually, an axial splitting, D_s, five times greater than the spin–orbit constant, λ (-103 cm^{-1} for the free Fe^{2+} ion[27]), qualitatively explains both the temperature dependence of ΔE_Q and the reduced low-temperature maximum.[28]

Reactions with Peroxide.—Since the aqua and chloro ligands in complexes **1**, **2** and **4** were found to be suitable for substitution by other monodentate ligands we tested their reaction with peroxides, in the hope of obtaining species of the type depicted by structure **I** in which an 'end-on' peroxide ligand is co-ordinated to either a Fe^{II} or Fe^{III} centre bound by a pentadentate ligand. The apparent stabilization of the Fe^{II} state by L^1 and L^2 was encouraging with respect to avoiding the formation of unwanted 'dead-end' oxo-bridged iron(III) complexes. It was desirable to characterize these putative peroxide adducts since they are most likely important intermediates in the catalysis reactions described later. Described below are our attempts to characterize the products of reactions between peroxides and complexes **1**, **2** and **4** in solution since we were unable to isolate any solid products.

Electronic spectra. Complexes **1** and **2** dissolved in acetonitrile or methanol react with hydrogen peroxide and *tert*-butyl hydroperoxide, to form brown species with absorption in the visible region at around 545 nm. In contrast, complex **4** when dissolved in methanol reacts with hydrogen peroxide to form a purple solution with an intense absorption at 537 nm ($\varepsilon = 750$ dm^3 mol^{-1} cm^{-1}). This absorption band is tentatively assigned to a peroxide-to-iron(III) charge transfer, in a complex in which the hydroperoxide is co-ordinated to iron(III) in an 'end-on' fashion (**I**). The purple species formed in the case of **4** slowly decays to a brown species at room temperature with a half-life of *ca.* 2 h. The UV/VIS spectra of a methanol solution of **4** with an excess of H_2O_2 is shown in Fig. 4. The purple peroxide species is transient and is eventually converted to a brown end product which we suspect to be of the same type as those formed from the reaction of complexes **1** and **2** with peroxides. In other words a similar peroxide adduct may be accessible for the iron complexes of L^1 however it is far too unstable to be observed, even at low temperatures. The ESR experiments described below support this explanation.

Mass spectrometry. The electrospray mass spectra of acetonitrile solutions of the two chloro complexes, **2** and **4**, mixed with aqueous solutions of hydrogen peroxide or *tert*-butyl hydrogen peroxide were recorded. We were unfortunately unable to identify any peaks attributable to species in which a dioxygen moiety is co-ordinated to LFe^{n+} ($n = 2$ or 3). Instead, the spectra indicate that the ligands are oxidized, m/z ratios corresponding to the loss of $NC_5H_4CH_2$ or $NC_5H_3(Me)CH_2$ sidearms and to the addition of an oxygen atom or hydroxyl group. We believe this result indicates that the pyridyl groups are oxidized to pyridyl *N*-oxides under the conditions of the mass spectrometry experiment. So even if a $LFe–O_2$ adduct is initially present this rapidly decomposes by oxidizing either an adjacent NC_5H_4/NC_5H_3Me moiety or another substrate in solution. These results contrast with the recent work of Sam *et al.*[5] who have been able to demonstrate the incorporation of two oxygen atoms derived from hydrogen peroxide into iron(III) bleomycin by means of electrospray mass spectrometry by mixing solutions of iron(III) bleomycin with solutions of H_2O_2 and $H_2{}^{18}O_2$. An important distinction between the present complexes and iron(III) bleomycin is the presence of the potentially oxidizable pyridyl donors in L^1 and L^2.

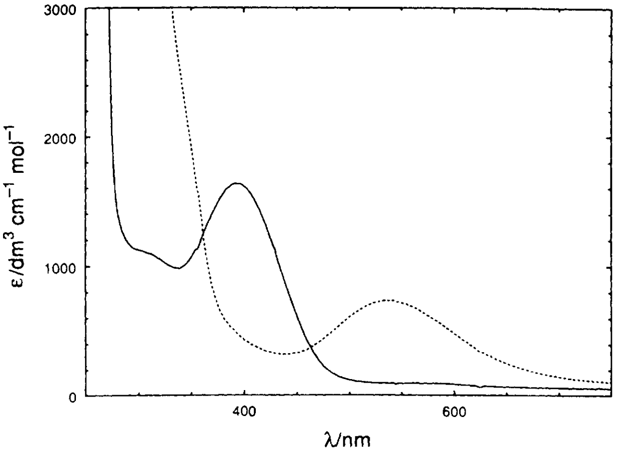

Fig. 4 The UV/VIS spectrum of $[FeL^2Cl]PF_6$ **4** in methanol (—) and after the addition of a slight excess of hydrogen peroxide (- - -)

EPR spectra. An aerated solution of **4** in methanol does not show any EPR features at 77 K. The addition of an excess of hydrogen peroxide gave an EPR spectrum indicative of the presence of low-spin Fe^{III}. Overlapping signals indicated the presence of two low-spin iron(III) species [Fig. 5(*a*)]. We assume the less intense signal to be due to an oxidized derivative of **4** and the more intense signal to be due to an iron(III) complex of L^2 with a co-ordinated peroxide ligand. In order to substantiate this proposal we used an alternative oxidizing agent. When **4** is treated with 1 equivalent of bromine ($E^\circ = 1.087$ V) at 0 °C followed by rapid cooling to 77 K, a low-spin rhombic Fe^{III} signal ($g = 2.30, 2.12, 1.92$) [Fig. 5(*b*)] and a weak high-spin Fe^{III} signal ($g = 4.11$) is observed. The low-spin signal is identical to the more rhombic signal in the hydrogen peroxide-oxidized compound. These features may be due to the formation of complexes of the type $[Fe^{III}L^2X]^{n+}$ ($n = 2$ or 3; X = Cl, Br, OH, MeO, H_2O or MeOH). When an excess of hydrogen peroxide was then added to the bromine-oxidized solution at 0 °C, a purple colour, characteristic for that we believe to be due to the peroxide derivative of FeL^2, developed. This solution gives an EPR spectrum similar to the spectrum observed in the first-mentioned EPR experiment *i.e.* when hydrogen peroxide is added to **4** without the intermediate step of oxidation with bromine [Fig. 5(*a*)]. Thus we propose that the rhombic EPR signal ($g = 2.19, 2.12, 1.95$) in Fig. 5(*a*) is due to the putative peroxo derivative *i.e.* $[FeL^2(OOH)]^{2+}$. This signal is typical for low-spin Fe^{III} and the values are similar to those of 'activated bleomycin'[30] ($g = 2.26, 2.17, 1.94$), which is believed to have an end-on hydrogen peroxide bound to a low-spin Fe^{III}-N_5 group. In activated bleomycin the nitrogen donor atoms are derived from two aliphatic, two imine and one deprotonated amide function, whereas in the present complex the N_5 co-ordination sphere consists of three imines and two aliphatic nitrogen functions. Presumably the most stable isomer has the peroxo group *trans* to one of the aliphatic nitrogen atoms. A similar arrangement has recently been suggested for 'activated bleomycin'.[30] Similar EPR parameters have been reported previously for other putative low-spin iron(III)–peroxo adducts with relatively simple ligands.[31]

The EPR spectra of solutions of the aqua complex **1** to which hydrogen peroxide had been added differ to those obtained for **4** above: on addition of hydrogen peroxide to a solution of **1** in acetonitrile a strong EPR signal at $g = 4.08$ and another weaker signal at $g = 2.18, 2.14, 1.93$ develops. A similar experiment to that described above for **4** in which bromine was added to a solution of **1** in acetonitrile in order to generate an oxidized species without peroxide gave a solution whose spectrum showed a very weak signal at $g = 4$. These results are not conclusive, but may suggest that an oxidized derivative of **1** *e.g.* of the form $[FeL^1X]^{n+}$ ($n = 2$ or 3; X = OH, H_2O or MeCN) in this case is a high-spin complex while the putative unstable peroxo derivative is a low-spin species.

Peroxidase Activity.—Complexes **1**–**4** were used as catalysts in a peroxidase assay using the peroxidase test substrate, abts [2,2′-azinobis(3-ethylbenzothiazoline-6-sulfonic acid)] and hydrogen peroxide in aqueous buffered solution, according to equation (1).

$$2H^+ + 2abts + H_2O_2 \longrightarrow 2abts^{\bullet +} + 2H_2O \qquad (1)$$

The radical cation $abts^{\bullet +}$, which is formed in the reaction exhibits a strong absorption band at 418 nm and the increase in absorption at this wavelength is a measure of peroxidase activity. The substrate was found to be oxidized in the presence of the iron complexes with up to 12 turnovers in 80 s. After this time the rate of oxidation slowed down perhaps because of catalyst inactivation. It was shown in a separate experiment that $abts^{\bullet +}$ could be reduced by **1** in a stoichiometric 1 : 1 reaction. In the light of this observation the apparent drop in activity can also be explained by an irreversible reaction of the oxidized substrate with the catalyst.

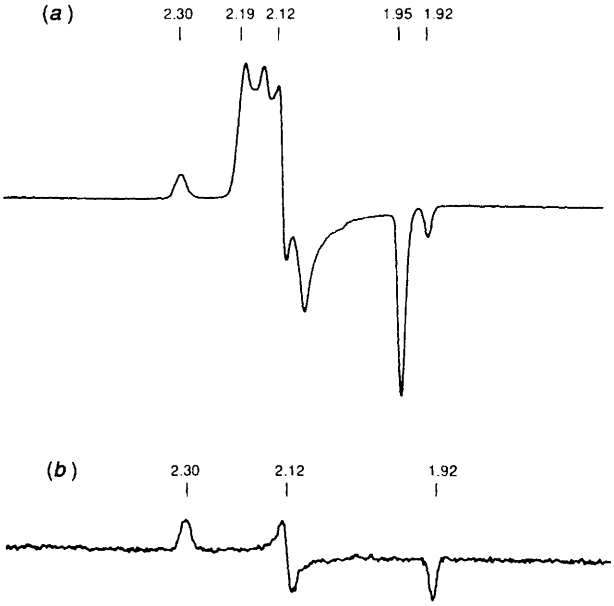

Fig. 5 The EPR spectrum of $[FeL^2Cl]PF_6$ **4** at 77 K (as frozen glass in methanol) plus (*a*) a slight excess of hydrogen peroxide (*b*) 1 equivalent of Br_2, spectrum expanded 10 × relative to the spectrum in (*a*). Two overlapping rhombic signals are present in (*a*). We assign these to a low-spin $Fe^{III}L^1(OOH)$ species with $g = 2.19, 2.12, 1.95$, and a low-spin $Fe^{III}L^1X$ species with $g = 2.30, 2.12, 1.92$. The signal in (*b*) is assigned to the latter $Fe^{III}L^1X$ species with $g = 2.30, 2.12, 1.92$. The g values are listed also above the spectra

4-Methoxybenzyl alcohol was shown to be oxidized to the corresponding aldehyde by hydrogen peroxide in the presence of complexes **2** and **4**. Low turnover numbers (three moles of product per mole catalyst) were found after 4 h and the yield was not further increased after 24 h. Again this can be explained by decomposition of the complexes as forecasted by electrospray mass spectrometry experiments, which showed that oxidation of the ligand (presumably *via* the formation of *N*-oxide species) was likely. If the oxidation of the substrate is slow, it is also possible that the catalyst is inactivated by reaction with the aromatic radical cation which is believed to be an intermediate in this type of reaction.[32] This is analogous with the observations for abts. Further studies to elucidate the oxidation mechanism are in progress.

Acknowledgements

This work is supported by grants from the Danish Natural Science Research Council (11-9227 to H. T. N. and 11-7916 to K. B. J.). We wish to thank T. Esbech and G. Bojesen for the electrospray mass spectra.

References

1 R. E. Stenkamp, *Chem. Rev.*, 1994, **94**, 715.
2 A. C. Rosenzweig, C. A. Frederick, S. J. Lippard and P. Nordlund, *Nature*, 1993, **366**, 537.
3 J. C. Boyington, B. J. Gaffney and L. M. Amzel, *Science*, 1993, **260**, 1482; W. Minor, J. Steczko, J. T. Bolin, Z. Otwinowski and B. Axelrod, *Biochemistry*, 1993, **32**, 6320.
4 D. H. Ohlendorf, J. D. Lipscomb and P. C. Weber, *Nature*, 1988, **336**, 403.
5 J. W. Sam, X.-J. Tang and J. Peisach, *J. Am. Chem. Soc.*, 1994, **116**, 5250.
6 N. Kitajima, H. Fukui and Y. Moro-oka, *J. Am. Chem. Soc.*, 1990, **112**, 6402; N. Kitajima, N. Tamura, H. Amagai, H. Fukui, Y. Moro-oka, Y. Mizutani, T. Kitagawa, R. Mathur, K. Heerwegh,

C. A. Reed, C. R. Randall, L. Que, jun. and K. Tatsumi, *J. Am. Chem. Soc.*, 1994, **116**, 9071.

7 Y. Zang, T. E. Elgren, Y. Dong and L. Que, jun., *J. Am. Chem. Soc.*, 1993, **115**, 811.

8 (*a*) J. S. Valentine, W. Nam and R. Y. N. Ho, in *The Activation of Dioxygen and Homogenous Catalytic Oxidation*, eds. D. H. R. Barton, A. E. Martell and D. T. Sawyer, Plenum, New York, 1993, pp. 183–198; (*b*) W. Nam, R. Ho and J. S. Valentine, *J. Am. Chem. Soc.*, 1991, **113**, 7052; (*c*) C. Sheu, S. A. Richert, P. Cofré, B. Ross, jun., A. Sobkowiak, D. T. Sawyer and J. R. Kannofsky, *J. Am. Chem. Soc.*, 1990, **112**, 1936.

9 H. Toftlund and S. Yde-Andersen, *Acta Chem. Scand., Ser. A*, 1981, **35**, 575.

10 TEXRAY-230, a modification of the SDP-Plus[11] set of X-ray crystallographic programs, Molecular Structure Corporation, College Station, TX, 1985.

11 SDP-Plus, the Enraf-Nonius Corporation X-ray diffraction data processing programs, College Station, TX, 1982.

12 R. B. Roof, *A Theoretical Extension of the Reduced Cell Concept in Crystallography*, Report LA-4038, Los Alamos Scientific Laboratory, NM, 1969.

13 D. T. Cromer and J. T. Waber, *International Tables for X-Ray Crystallography*, Kynoch Press, Birmingham, 1975; vol. IV, Tables 2.2.8. and 2.3.1., for the scattering factor curves and the anomalous dispersion values, respectively.

14 The NRCVAX Crystal Structure System, A. C. Larson, F. L. Lee, Y. Le Page, M. Webster, J. P. Charland and E. J. Gabe, as adapted for PC use by Peter S. White, University of North Carolina, Chapel Hill, NC, 1990.

15 F. Varret, *Proceedings of the International Conference on Mössbauer Effect Applications*, Jaipur, 1981. Indian National Science Academy, New Delhi, 1982.

16 J. S. Shindler, R. E. Childs and W. G. Bardsley, *Eur. J. Biochem.*, 1976, **65**, 325.

17 H.-R. Chang, J. K. McCusker, H. Toftlund, S. R. Wilson, A. X. Trautwein, H. Winkler and D. N. Hendrickson, *J. Am. Chem. Soc.*, 1990, **112**, 6814.

18 F. König, *Prog. Inorg. Chem.*, 1987, **35**, 527.

19 M. Mikami, M. Konno and Y. Saito, *Chem. Phys. Lett.*, 1979, **63**, 566.

20 G. Vos, R. A. G. De Graaf, J. G. Haasnoot, A. M. Van der Kraan, P. de Vaal and J. Reedijk, *Inorg. Chem.*, 1984, **23**, 2905; W. H. Baur, *Acta Crystallogr.*, 1962, **15**, 815.

21 C. K. Jørgensen, *Oxidation Numbers and Oxidation States*, Springer Verlag, Berlin, 1969.

22 E. E. Mabbs and D. J. Machin, *Magnetic and Transition Metal Complexes*, Chapman and Hall, 1973.

23 N. N. Greenwood and T. C. Gibbs, *Mössbauer Spectroscopy*, Chapman and Hall, New York, 1971.

24 P. Garge, R. Chikate, S. Radhye, J.-M. Savariault, P. de Loth and J.-P. Tuchagues, *Inorg. Chem.*, 1990, **29**, 3315; D. Boinnard, P. Cassoux, V. Petrouleas, J.-M. Savariault and J.-P. Tuchagues, *Inorg. Chem.*, 1990, **29**, 4114.

25 J. R. Sams and T. B. Tsin, *Inorg. Chem.*, 1975, **14**, 1573.

26 A. Ducouret Céréze and F. J. Varret, *J. Phys. Fr. (Paris)*, 1988, **49**, 661.

27 R. E. Tress, *Phys. Rev.*, 1951, **82**, 683.

28 R. Ingalls, *Phys. Rev.*, 1964, **133**, A787.

29 R. M. Burger, J. Peisach and S. B. Horwitz, *J. Biol. Chem.*, 1981, **256**, 11636.

30 R. J. Guajardo, J. D. Tan and P. K. Mascharak, *Inorg. Chem.*, 1994, **33**, 2838.

31 Y. Nishida and N. Tanaka, *J. Chem. Soc., Dalton Trans.*, 1994, 2805; S. Ménage, E. C. Wilkinson, L. Que, jun. and M. Fontecave, *Angew. Chem., Int. Ed. Eng.*, 1995, **35**, 203; A. Sauer-Masarwa, N. Herron, C. M. Fendrick and D. H. Busch, *Inorg. Chem.*, 1993, **32**, 1086.

32 B. Menuier and G. Labat, *Bull. Soc. Chim. Fr.*, 1990, **127**, 553.

Received 1st *June* 1995; *Paper* 5/03504J